Full-Polarization Imaging of PolConverted VLBI Observations
From Black Hole Images with the EHT to AGN Jets with VGOS

I. Martí-Vidal[1], V. Pérez-Díez[2], E. Albentosa-Ruíz[1]

Abstract The VLBI Global Observing System (VGOS), developed by the International VLBI Service for Geodesy and Astrometry (IVS), uses receivers with a very wide spectral range, able to cover simultaneously from S (2 GHz) to X (12 GHz) bands. These receivers are designed in a linear polarization basis, in order to achieve a high polarization purity across the whole VGOS band with a minimum cost. This paper delves into the intricacies of the VGOS data calibration, including the conversion from linear to circular polarization using the PolConvert algorithm. We also discuss the performance of PolConvert applied to other astronomical interferometers (like the Event Horizon Telescope, EHT), which resulted in the first (polarized) images of black holes. We show how the polarization signal of the EHT is an independent robust proof of the ring-like images of M 87* and Sgr A*. Finally, we present the first results obtained with a Wide-Band Global Fringe-Fitting (WB-GFF) algorithm applied to a VGOS dataset, comprising eight antennas with intercontinental baselines. The advantages of a Global Fringe-Fitting with respect to the typical baseline-based solutions are also discussed.

Keywords VLBI, VGOS, Polarization

1. Dpt. Astronomia i Astrofísica (Univ. Valencia, Spain). Observatori Astronòmic (OAUV, Univ. Valencia, Spain)
2. Observatorio Astronómico Nacional (OAN/IGN, Madrid, Spain)

1 Introduction

Wide-band receivers in Radio Astronomy (with fractional bandwidths of the order of 100%) are usually designed to observe in a linear polarization basis, due to several reasons. For instance, the sensitivity of linear-polarization receivers is slightly higher (because there are fewer lossy optical components along the signal path), the costs are cheaper, and the instrumental polarization is notably lower (because the hardware-based polarization conversion into a circular basis has a peak performance only on a finite bandwidth).

However, circular-polarization receivers have historically been the preferred choice in Very Long Baseline Interferometry (VLBI), mainly due to the much easier (and better) calibration procedure. The long baselines involved in VLBI introduce different parallactic angles at each station. If the observations are taken in a circular polarization basis, the different parallactic angles can be simply absorbed as a *deterministic phase correction* before the fringe fitting. On the contrary, if linear polarizers are used in VLBI, all the instrumental (and frequency-dependent) phases and amplitude gains, relative between polarization channels, must be known for all antennas before *any* other calibration quantity can be derived or applied (including the parallactic angle, which has to be corrected before the fringe fitting). Such a limitation makes the calibration of VLBI with linear polarizers a more computationally expensive and complicated task.

Nonetheless, there are remarkable cases of VLBI stations with linear-polarization receivers, like the Atacama Large Millimeter/sub-mm Array (ALMA) in its *phasing mode*, developed by the ALMA Phasing Project (APP) for the use of ALMA as a VLBI station (e.g., [16]). Thanks to this phasing mode, ALMA

became the most sensitive VLBI station of the Event Horizon Telescope (EHT) and the Global mm-wave VLBI Array (GMVA), observing at 230 GHz and 86 GHz, respectively [16].

The ALMA receivers are designed in linear polarization, whereas the rest of the EHT and GMVA stations register their signals in a circular polarization basis. Such a mixture of different polarizations within the same interferometer (ALMA + VLBI) is corrected with the program *PolConvert* [15], which performs a post-correlation conversion of the visibilities into a pure circular basis. The final product of PolConvert is a new VLBI dataset, written as if ALMA would have observed using pure circular-polarization receivers.

The PolConvert algorithm (based on the Radio Interferometry Measurement Equation, RIME; [21]) is relatively simple. Indeed, soon after its implementation for ALMA-VLBI, a new version of PolConvert was developed for its use with the VLBI Global Observing System (VGOS). The idea behind this new version was to perform a post-correlation conversion of the VGOS data (e.g., [2]) as a way to optimize the calibration quality (and efficiency) of VGOS, as well as to allow for astronomical exploitation of the data in full polarization.

In these proceedings, we will summarize some of the main results of PolConvert. First, we will briefly discuss the EHT observations of M87*. Then, we will discuss an epoch of VGOS observations, where we show the performance of PolConvert when all the observing stations are equipped with linear-polarization receivers. We will also present a Wide-Band Global Fringe Fitting algorithm that, combined with the PolConversion, allows us to obtain wide-band full-polarization images of the AGN observed with VGOS.

2 Astronomical Results with PolConvert

Figure 1 (top left) shows the cross-polarization frequency-dependent gains of ALMA (and two other stations) in the EHT observations of April 11, 2017 [7]. This ALMA calibration information is used by PolConvert to rewrite the EHT data in a pure circular basis, whereas the cross-pol gains of the other antennas are just related to the calibration of the absolute polarization angle [7]. Some examples of PolConverted visibility peaks are shown in the same figure (top right), for the baseline between ALMA and IRAM-30m (Pico Veleta, Spain). The cross-hand correlation peaks (i.e., *RL* and *LR*, related to the polarized intensity of the observed source), are clearly weaker than the parallel-hand correlations (i.e., *RR* and *LL*, related to the total intensity). Similar results are obtained for all the other ALMA-related baselines and scans. Weak cross-hand correlations (compared to the parallel-hand ones) in all baselines and for all scans are a good indication of a successful PolConversion.

Figure 1 (bottom left) shows the polarized image of M87*, published by the EHT Collaboration in [7] for the observations taken on April 11, 2017. The image shows the electric vector position angles (EVPA) as "wind lines", with a contrast locally proportional to the polarized intensity. It is very remarkable (and this is indeed an important astrophysical finding) that the EVPA roughly follows the orientation of the ring (i.e., the "wind lines" rotate following the ring position angle and generating a spiral-like pattern). A similar qualitative EVPA structure has also been found in the black hole of our Galactic Center, Sgr A* [8].

It must be noticed that the EVPA structure shown in Figure 1 (bottom left) has not been directly probed by the interferometer. These EVPAs are rather computed from images of the Stokes parameters Q and U (i.e., Figure 1, bottom right), which are the quantities directly appearing in the interferometer's visibility matrix [21]. The Q and U images are produced with the *same* calibration gains that were used to generate the total-intensity image (i.e., Stokes I) and processed, pixel by pixel, to compute the EVPAs using the non-linear function

$$\mathrm{EVPA} = \frac{1}{2}\arctan\left(\frac{U}{Q}\right). \qquad (1)$$

An EVPA distribution that tightly follows the orientation of the total-intensity ring (Figure 1, bottom left), cannot be produced by a mere instrumental effect. The non-linear combination of Q and U given in Equation 1 is an observational quantity completely unrelated to the total-intensity brightness distribution. Hence, such an agreement between both quantities (total-intensity ring and EVPA rotation) must be intrinsic to the source (i.e., not produced by any PSF or calibration-like artifact). Polarimetry is, thus, the ultimate proof of the fidelity of the ring-like EHT images of M87* (and SgrA*).

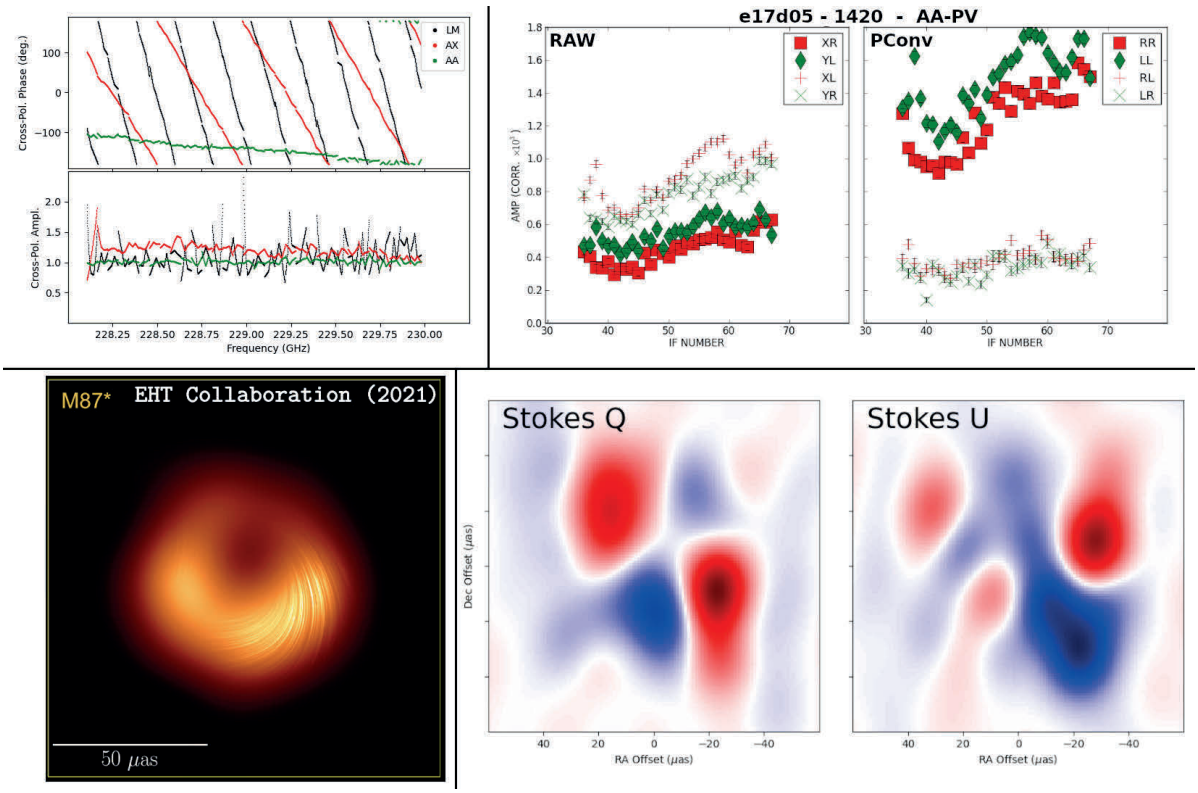

Fig. 1 **Top left**, cross-polarization bandpasses for three EHT antennas (ALMA in green, APEX in red, and the LMT in black), derived by PolConvert for an epoch of observations in year 2017. **Top right**, fringe peaks for the baseline between ALMA (code AA) and IRAM-30m (code PV), of a scan on 3C 279; the raw data (i.e., in a mixed linear-circular polarization basis) are shown at left; the PolConverted (i.e., pure circular) data, at right. **Bottom left**, polarized image (in "wind plot" format) of M87* for April 11, 2017, as published in [7]. **Bottom right**, corresponding images in Stokes Q and U; red and blue colors correspond to positive and negative intensities, respectively.

3 PolConvert Applied to VGOS

PolConvert is able to determine the cross-polarization gains of any VLBI station with linear-polarization receivers, using an algorithm called *Global Cross-Polarization Fringe Fitting* [15]. These gains are needed for a successful conversion into a circular basis. When applied to VGOS observations, PolConvert produces multi-band cross-polarization delays with very clear peaks, which remain remarkably stable across weeks (Figure 2, left) or even years (e.g., [10, 17]) with very few exceptions.

Once the VGOS data are PolConverted, it is possible to apply the parallactic-angle corrections directly to the visibilities, as an a-priori correction, so that we can combine the parallel-hand correlations (*RR* and *LL*) coherently and generate one single product with all the Stokes *I* signal in it. Having Stokes *I* in one single correlation product makes the fringe-fitting calibration much more efficient, saving time and memory.

In [17], we present the results of a complete PolConversion and calibration of a global 24-hour VGOS session of observations (VO2187, observed on 6−7 July, 2022). In that publication, it is shown that running PolConvert on a 24-hour experiment produces circular-polarization visibilities with a high quality, from which it is possible to generate full-polarization images of the observed AGN. In the following subsections, we summarize the main results obtained for session VO2187.

3.1 Wide-Band Global Fringe Fitting

Geodetic VLBI observations are usually fringe-fitted independently for each baseline. This approach is his-

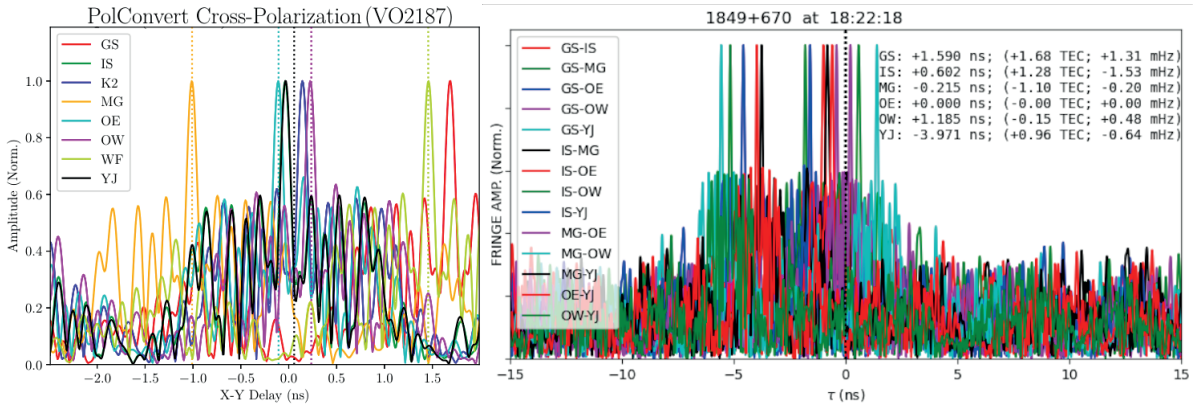

Fig. 2 **Left**, cross-polarization delays of VGOS antennas, as estimated by PolConvert at the epoch of session VO2187 [17]. Dotted lines mark the cross-polarization peaks estimated at another epoch [10] for the antennas commonly observing in both experiments. **Right**, multi-band delay fringes of the (PolConverted) Stokes *I*, for all the baselines in a scan of VO2187. The fringes are fitted to a global (i.e., antenna-based) wide-band gain model, consisting of non-dispersive (i.e., troposphere) and dispersive (i.e., ionosphere) corrections. The residual gains for each antenna (Onsala East (OE) being the reference station) are shown at the top right corner.

torically preferred for Geodesy, because the time stamp of each observation used in the geodetic model is referred to the exact time of arrival of the sky signal to the first antenna of each baseline. Hence, each baseline has a slightly different time stamp for the same set of VLBI observations (i.e., for the same *scan*), making a separate baseline fringe-fitting a reasonable approach.

On the contrary, astronomical VLBI uses the same time stamp for all the visibilities observed in the same scan. To make this possible, a common reference frame (e.g., the Earth center) has to be used for the timing of all baselines. This is the only way to properly *close* the closure quantities that encode information about the brightness distribution of the observed sources. Actually, the VLBI correlation software DiFX [6], used in VGOS, refers the scan times to the Earth center, and it is only when the (already fringe-fitted) data are exported to VGOS-DB format (or equivalent) that the time stamps of the visibilities are re-computed to the Geodesy standard with the help of the Earth rotation model used in the correlation.

In the case of a common time for all baselines in a scan, a *global* calibration approach is preferred, because it keeps (by definition) all the closure-based source information, which can then be turned into images with the help of deconvolution algorithms. A global calibration approach parameterizes the gains as antenna-based quantities. For a given scan, there are as many fringes as baselines, N_b, a number that depends quadratically on the number of antennas, N_a, via the well-known relation

$$N_b = N_a(N_a - 1)/2. \quad (2)$$

Therefore, the number of fitting (gain) parameters in a global calibration (which goes as N_a) is much smaller than in a baseline-based calibration. A lower number of parameters means a faster and more efficient fitting, which also decouples better the source-dependent information from the antenna-based quantities.

In Figure 2 (right), we show all the multi-band fringes in a scan of VO2187. There is a total of six antennas and 14 baselines in the scan (we are not using the intra-site baseline between the twin Onsala stations, OE−OW, which is heavily affected by common RFI and phase-cals). All the fringes are satisfactorily modeled with the global solutions printed at the top right corner of the plot (we use OE as the reference station). The global quantities shown are residuals with respect to the correlator model and the prior ionospheric correction derived from IONEX maps (see [17] for more details).

3.2 Full-Polarization Images from VGOS

Once the Wide-Band Global Fringe Fitting is finished for all the scans, an a-priori amplitude calibration is performed, based on system temperatures and approx-

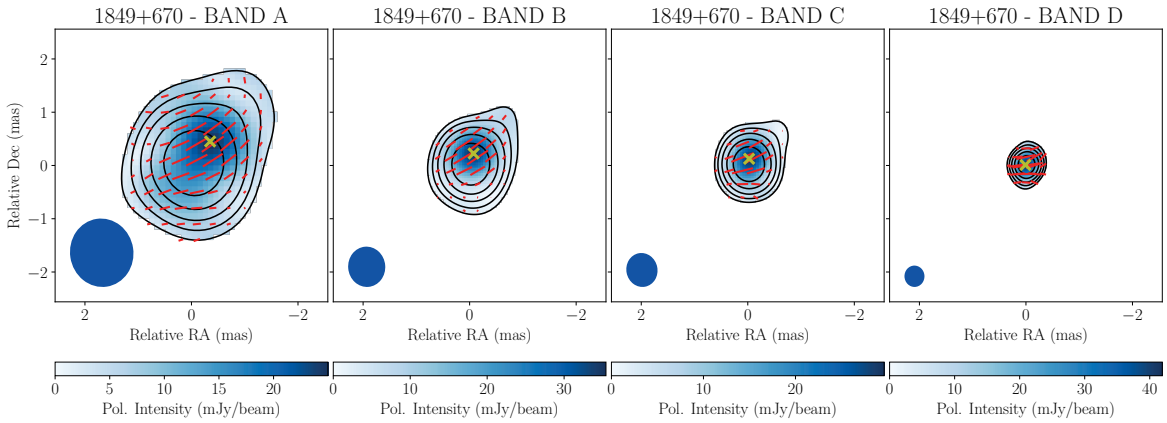

Fig. 3 Full-polarization images of source 1849+670, observed with VGOS at the epoch of session VO2187 [17]. Frequency increases from left to right ($\sim$ 2, 5, 6, and 11 GHz). Black contours mark the total intensity; blue colors, polarized intensity; and red lines, the polarization angles (EVPAs), with lengths proportional to the polarized intensity. The full width at half maximum (FWHM) of the convolving beam at each band is shown at the bottom left corner of each plot. The yellow crosses mark the location of the polarization peak at each band. The images are centered at their total-intensity peaks.

imated antenna gains in a subset of the VGOS array. Then, a process of hybrid imaging (involving the self-calibration of antenna-based phase gain residuals and amplitude corrections) is executed on a set of sources with sufficient UV coverage [17], and, finally, full-polarization images are generated. We show a sample set of polarization images in Figure 3. The brightness distributions taken from these images can later be included in the Fringe-Fitting model, thus refining the calibration and producing antenna-based solutions virtually free from contamination related to the source structures and suited for their use in Geodesy analysis (although with some peculiarities that still have to be taken into account, as we discuss in the next section).

4 Current Limitations and Future Plans

Besides allowing for the astronomical exploitation of the VGOS observations, the other objective of our calibration procedure is to provide an alternative (and ideally faster and more robust) way of generating datasets ready for geodetic analysis, taking advantage of the global (antenna-based) parametrization of the fringe solutions free from any source-structure (and source-polarization) effects. To achieve this objective, several issues still have to be fixed and understood, as we summarize in the following lines.

4.1 Source Structure and Global Fringe Fitting

The source structure can become a severe limiting factor for the precision and accuracy of geodetic observations (e.g., [22, 23]). In astronomical VLBI, accounting for the source-structure effects in the gain calibration is a relatively well-established standard procedure (e.g., [20]). In the Global Fringe Fitting approach, the observed (uncalibrated in phase) visibilities are just divided by the Fourier transform of the source brightness distribution, hence removing the whole source structure from the data in one single step[1]. Then, the antenna gains are adjusted to match the ratio of observed-to-model visibilities by assuming a centered point source. The final results of this process are refined antenna-based gains, with the property of referring the source astrometry to the phase center of the model image.

This procedure has been successfully used in multiple astronomical works, either involving phase-referencing calibration or differential phase-delay astrometry (e.g., [13, 14]). In principle, including the very same procedure into the Wide-Band GFF that we have implemented for VGOS [17] should be immediate. However, the wide fractional bandwidth of

[1] Alternatively, the amplitude information can be removed from the fitting by just computing the phase difference between visibilities and model, instead of the ratio of complex values.

VGOS is the cause of new effects related to the source structure that have to be properly understood before doing so: *the frequency dependence of AGN images*.

4.2 Core Shift

The spectral index of an AGN jet is not constant along the jet stream. The spectrum is usually flatter (or even inverted) at regions close to its base (i.e., close to the black hole, where magnetic-field gradients and particle densities are higher) and becomes steeper (i.e., optically thin) downstream (e.g., [4]). Such a frequency dependence may induce a delay that has nothing to do with the Earth geometry and depends on each baseline (in essence, the delay increases as the baseline aligns more with the jet direction). Unfortunately, this jet-induced delay cannot be estimated with a mere model image at a given frequency; a more elaborated multi-frequency jet model is needed for this (e.g., [22]).

Fortunately, for the case of AGN jets that fulfill some restrictions (i.e., a conical shape and a perfect energy equipartition between plasma particles and magnetic fields), it has been shown that the net effect of the jet spectral dependence on the measured delay is always null [19]. The bad news is that not all the AGN jets obey these special restrictions. Actually, only a small fraction of the AGN jets seem to do so (e.g., [12]), although the delays caused by departures from energy equipartition are usually *small*.

In any case, even if the frequency effects of the jets are small, they are still non-zero. A study at the level of the VGOS precision (the picosecond level) is definitely needed. In the case of AGN with prominent jets, multi-frequency-synthesis (mfs) algorithms can be used to reconstruct frequency-dependent source models and subtract their effects from the VGOS observables. However, for sources with weak jets or unresolved structures (which is usually the case for the *defining* ICRF sources) there is no way to determine the spectral dependence of the AGN brightness distributions using ordinary VGOS observations. More elaborated (e.g., phase-referencing) observations strategies are required.

4.3 From Global to Baseline-Based

Global Fringe Fitting uses all the available information of each scan, in order to find self-consistent antenna-based quantities able to optimally model the fringe residuals seen at all baselines. The parameter space to be probed in a global fit is much smaller than in the case of baseline-based solutions (Equation 2) and produces antenna-based quantities that are virtually free from the source-dependent closure quantities (the closure phases are kept in the post-fit fringe residuals, which are the quantities used by the astronomers for their source imaging).

However, modeling the fringe residuals as antenna-based quantities has the unavoidable effect of creating covariance among the model predictions of different baselines that share a common antenna. And this covariance may affect the fitting of the geodetic models, which may assume that each VLBI observation (i.e., each baseline at each scan) is statistically independent from the others.

Properly accounting for the covariance induced among baselines by a global gain parameterization is something that still has to be studied. Moreover, the relative weights of the solutions for each baseline have to be estimated from the antenna-based quantities, which again depends on the whole covariance matrix.

Last but not least, the global solutions are computed using the same time reference for all baselines, whereas the baseline-based solutions in a Geodetic fitting use the time of arrival of the signal to the first antenna of each baseline (i.e., the signal arriving at any given antenna may have several different time stamps, depending on the other antennas that form baselines with it). Fortunately, such a conversion is already being done by the standard software used to produce vgosDb from the HOPS calibration [3]; adapting it to our software should not be difficult.

5 Conclusions

We have briefly presented a calibration procedure of VGOS observations different from the official pipeline developed by the MIT Haystack Observatory. This procedure makes use of the program *PolConvert* to rewrite the correlation products in a circular polarization basis, hence allowing us to employ simpler VLBI cal-

ibration strategies and obtain full-polarization source information using standard VLBI polarimetry algorithms.

We have summarized some of the main results of PolConvert when applied to different VLBI arrays (on the one hand, the EHT observations of M87* in 2017; on the other hand, a VGOS array of eight stations observing in a global 24-hour epoch).

Regarding M87* (and similar to SgrA*), the sensitive ALMA-related PolConverted baselines of the EHT allowed the EHT Collaboration to obtain EVPA images that rotate in a tight relation to their position angles along the ring-like images (Figure 1, bottom left). Such a behavior cannot be produced by any PSF or calibration-like artifact, given that the EVPA is computed from the non-linear combination of other images (Stokes Q and U) that are independent of Stokes I. Polarimetry is thus the ultimate proof of the fidelity of the ring-like EHT images of M87* and SgrA*.

Regarding VGOS, we have successfully PolConverted a complete 24-hour experiment with eight antennas and intercontinental baselines. We have also performed a Wide-Band Global Fringe Fitting on the whole dataset, correcting for dispersive and non-dispersive atmospheric delays. These global solutions (which preserve the phase closures for all sources across the whole VGOS band) allow us to obtain full-polarization images (we show an example in Figure 3). Having complete model images for all the observed sources would make it possible to remove the structure effects from the geodetic observables, bringing the maximum precision and accuracy to VGOS. However, there are effects that still have to be understood regarding the source structure, in particular the frequency dependence of the jet brightness distributions.

Acknowledgements

This work has been supported by Projects PID2022-140888NB-C22 (from MICINN) and ASFAE/2022/018 (from GVA).

References

1. Akiyama K., Ikeda S., Pleau M., et al. 2017, AJ, 153, 159
2. Aleff et al., *The EUropean-VGOS Project*, in Proceedings of the 24th EVGA Meeting, March 2019, Las Palmas, Spain
3. Barrett J., Capallo R., Corey B., et al. 2021, *VGOS Data Processing Manual, v1.11*, https://www.haystack.mit.edu
4. Blanford R. D. & Koenigl A. 1979, ApJ, 232, 34
5. Broderick A. E., Gold R., Karami M., et al. 2020, ApJ, 897, 139
6. Deller A. T., Tingay S. J., Bailes M. & West C. 2007, PASP, 119, 853
7. EHT Collaboration et al. 2021, ApJL, 910, 12
8. EHT Collaboration et al. 2024, ApJL, 964, 2
9. Högbom J. A. 1974, A&AS, 15, 417
10. Jaron F., Martí-Vidal I., Schartner M., et al. 2024, RaSc, 59, 4
11. Chael A. A., Johnson M. D., Narayan R., et al. 2016, ApJ, 829, 11
12. Kovalev Y. Y., Lobanov A. P., Pushkarev A. B., et al. 2008, A&A, 483, 759
13. Martí-Vidal I., Marcaide J. M., Alberdi A., et al. 2011, A&A, 533, 111
14. Martí-Vidal I., Marcaide J. M., Guirado J. C., et al. 2008, A&A, 478, 267
15. Martí-Vidal I., Roy A., Conway J. & Zensus A. J. 2016, A&A, 587, 143
16. Matthews L. D., Crew G. B., Doeleman S. S., et al. 2018, PASP, 130 5002
17. Pérez-Díez V., Martí-Vidal I., Albentosa-Ruíz E., et al. 2024, A&A, accepted
18. Pesce D. W. 2021, AJ, 161, 178
19. Porcas R. W. 2009, A&A, 505, 1
20. Schwab F. R. & Cotton W. D. 1983, AJ, 88, 5
21. Smirnov O. M. 2011, A&A, 527, 106
22. Xu M. H., Savolainen T., Anderson J. M., et al. 2022, A&A, 663, 83
23. Xu M. H., Savolainen T., Zubko N., et al. 2021, JGRB, 126, 4